General Disclaimer

One or more of the Following Statements may affect this Document

- This document has been reproduced from the best copy furnished by the organizational source. It is being released in the interest of making available as much information as possible.

- This document may contain data, which exceeds the sheet parameters. It was furnished in this condition by the organizational source and is the best copy available.

- This document may contain tone-on-tone or color graphs, charts and/or pictures, which have been reproduced in black and white.

- This document is paginated as submitted by the original source.

- Portions of this document are not fully legible due to the historical nature of some of the material. However, it is the best reproduction available from the original submission.

NASA TECHNICAL MEMORANDUM

NASA TM X-73499

NASA TM X-73499

TOWARD MORE ENVIRONMENTALLY RESISTANT GAS TURBINES: PROGRESS IN NASA-LEWIS PROGRAMS

by Carl E. Lowell, Salvatore J. Grisaffe and Stanley R. Levine
Lewis Research Center
Cleveland, Ohio 44135

TECHNICAL PAPER to be presented at the
Third Conference on Gas Turbine Materials
in a Marine Environment
Bath, England, September 20-23, 1976

TOWARD MORE ENVIRONMENTALLY RESISTANT GAS TURBINES: PROGRESS IN NASA-LEWIS PROGRAMS

by Carl E. Lowell, Salvatore J. Grisaffe and Stanley R. Levine

Lewis Research Center

ABSTRACT

The Lewis Research Center is conducting a wide range of programs for improving the environmental resistance to oxidation and hot corrosion of gas turbine and power system materials. They range from fundamental efforts to delineate attack mechanisms, allow attack modeling and permit life prediction, to more applied efforts to develop potentially more resistant alloys and coatings. This paper surveys some of the recent results of these programs.

Oxidation life prediction efforts have resulted in a computer program, "COREST", which provides an initial method for predicting long time metal loss using short time oxidation data by means of a paralinear attack model. While this early effort centered on isothermal oxidation coupled with oxide vaporization, "COREST" is now being expanded to include oxide spallation. This more closely approaches the situation in real turbines on heat-up and cool down. The factors governing oxide spallation and their relative magnitude are also under investigation to allow further refinement of "COREST" with a more accurate oxidation attack model. In this regard work has been performed to determine the role of coefficient of thermal expansion (CTE) mismatch on oxide spallation. Also, supplemental efforts on measuring and evaluating CTE have resulted in the development of a novel mathematical treatment in which CTE can be expressed by a single constant. A paralinear oxidation attack model in conjunction with regression analysis of weight change data has been used to treat oxidation and hot corrosion attack of a number of alloys in the Ni-Cr-Al system. This approach resulted in compositional maps on which oxide spall resistance is estimated so as to guide alloy and coating development.

Efforts in alloy development have centered on oxide-dispersion strengthened (ODS) alloys based on the Ni-Cr-Al system. Compositions have been identified which are compromises between oxidation and thermal fatigue resistance. The Ni-Cr-Al system has also formed the basis for coatings on the new γ/γ'-δ alloys. These coatings improve not only alloy oxidation resistance, but also provide superior thermal fatigue resistance. Another area of oxidation research deals with NASA's efforts in exploring the oxidation resistance of NiCrAlY-MgO cermets. These mixtures of alloy and ceramic are being examined to provide desired combinations of abrasion resistance and oxidation resistance.

Fundamental studies of hot corrosion mechanisms include thermodynamic studies of sodium sulfate formation during turbine combustion. In order to generate reliable data, information concerning species formed during the vaporization of Na_2SO_4 has been developed using high temperature mass spectrometry. The vapor species and their vapor pressures have been determined. As a result of these studies, equilibrium flame compositions have been calculated and are in the process of being experimentally verified. In the area of more applied hot corrosion research, several aluminide coatings have been tested in hot corrosion using Mach 0.3 burner rig test facilities. The results of this work indicated that for coatings of a given type, resistance was related more to the thickness of the coating than to its exact aluminide or substrate alloy composition. Also determined in burner rig testing was the efficiency of a Cr bearing fuel additive in retarding hot corrosion. While the additive reduced hot corrosion attack by a factor of two, it did not eliminate hot corrosion nor did it appear to change the attack mechanism. This was especially true in tests involving

many heating-cooling cycles (one cycle per hour). Finally, attempts to reduce the hot corrosion of current turbine alloys by alloying have met with only modest success. Si additions to B-1900 resulted in somewhat improved resistance to hot corrosion but only at the expense of some loss of mechanical properties.

INTRODUCTION

Oxidation, corrosion, and erosion can be major factors in reducing the life of gas turbine engine components. Considerable improvement in the corrosion resistance of cast conventional superalloys used for turbine blades and vanes has been made by alloy modification and by coating. However, as higher temperature advanced materials--directionally strengthened, oxide dispersion strengthened, etc.,--have been introduced to increase engine performance and/or extended component life, such long time, high temperature environmental resistance becomes harder to achieve.

This paper presents highlights from some of the recent NASA-Lewis Research Center materials programs which are directed toward understanding and minimizing environmental attack. These efforts range in scope from fundamental studies of attack mechanisms through the development of components aimed at improving the performance of specific engines. In light of the focus of this conference, emphasis will be placed on those results dealing with understanding attack mechanisms and with ways to minimize such attack.

ENVIRONMENTAL ATTACK

Engine materials must have adequate resistance to the anticipated engine environment. However, few laboratory studies have examined material behavior under appropriate conditions of pressure, temperature, cycling, and environment for times approaching actual engine life. For this reason there is a real need to develop the methodology necessary to estimate attack at times and conditions beyond those of the laboratory test. Some of the general Lewis efforts in attack estimation were reported to this group at the 1972 Conference (ref. 1). An initial step estimating oxidation attack was reported at the 1974 Conference (ref. 2) where a mass balance approach was used to calculate net sample weight change (net sample weight change = k(weight retained oxide)-m(weight oxide spalled)).

More recently, a tentative oxidation model based on paralinear weight change behavior has been coupled with a FORTRAN computer program called "COREST"--Corrosion Estimation (ref. 3). This model assumes parbolic growth of the oxide combined with a linear loss via vaporization. The weights of the retained oxide and the amount of metal consumed can be calculated from specific weight change data assuming that the type of oxide which formed is known. An example of the prediction capability for the isothermal oxidation of Ni-40Cr at 1200° C is shown in figure 1. The input for this calculation was the maximum weight gain (W) and the time at which this maximum was reached. Figure 2 shows the calculated amounts of metal consumed for a number of Cr_2O_3 forming alloys oxidized isothermally at 1150° C for long times. These calculations show that for long life components, metal consumption calculations based on the less accurate parabolic oxidation model (solid line) can be in great error and such an extrapolation can indicate consumption rates much slower than are actually occurring. COREST can also be used in cyclic oxidation studies where the spalling rate appears relatively uniform from cycle to cycle.

The amount of oxide formed and the amount of oxide that spalls off on each thermal cycle has a major effect on the magnitude of the amount

of metal consumed during oxidation. Thus, a knowledge of the factors involved in oxide spallation is important to the development of an accurate degradation model. One such factor is the difference between the exposure temperature and the temperature to which the material cools on each cycle--defined here as ΔT. A continued effort has been devoted toward examining the influence of ΔT on spalling (ref. 4). Figure 3 shows some of the results of that study conducted on a variety of alloys. In the plot shown, which is the specific weight change versus ΔT, it appears that most alloys have a minimum ΔT, it appears that most alloys have a minimum ΔT which must be exceeded before spalling can be observed. The complex oxide forming alloys show significant weight losses even when the ΔT is 800° C. The nickel alloys that primarily form aluminum oxide scales, e.g., TDNiCrAl, must experience 1000° to 1200° C ΔT to develop such spalling. However, the FeCrAl alloy, with a 40% lower coefficient of thermal expansion, was spall resistant over the entire range of cooling in this study (1200° C exposure to -200° C in liquid nitrogen).

Since CTE appears to be an important factor in oxide spalling, there was a need to express this property in a tractable form that allowed a simple comparison of one alloy to another over a broad range of temperatures. An equation was developed (ref. 5, fig. 4) for nickel- and cobalt-chromium-aluminum alloys that expresses thermal expansion by means of a single expansion constant, R, related to lattice parameter and temperature and defines the shape of the curve. The normally used mean CTE is merely a value of expansion at any one T and gives no indication of curve shape while change in length/original length ($\Delta L/L$) plots are cumbersome because they require the use of a number of constants for curve fitting. Table I gives a more complete presentation of the NiCrAl expansion data. The expansions of both the gamma and gamma prime phases were shown by a statistical analysis of these data to be about equal to each other and to that of the beta aluminide phase. Also noted was the lower expansion of the alpha chromium phase. Table I data when analyzed statistically further shows that there was no significant variation in the values of R within any one phase as a function of composition.

The parallinear oxidation model approach was used to analyse the cyclic oxidation behavior of alloys in the NiCrAl system at 1100 and 1200° C. An attack parameter (ref. 6) was developed from the paralliner model equation as shown in figure 5. This parameter was then fitted to an estimating equation as a function of Cr and Al content by multiple linear regression. These equations can then be represented pictorially as iso-attack contours on ternary phase diagrams at each test temperature. These were computer plotted directly from the estimating equations. The regression analysis of the attack parameter data also indicated that Cr or zirconium oxide pickup from the melting crucible significantly improved the oxidation resistance of alloys in the Ni-50Cr-50Al system as reflected by significant lowering of the attack parameter. Those results are shown in figures 6 and 7. The value of the attack parameter approach is that it permits comparisons of a quantitative nature over a broad range of compositions and test conditions.

A knowledge of the cyclic oxidation behavior of NiCrAl alloys has considerable practical value. First, they are being considered for use as the matrix metal for oxide dispersion strengthening to make high temperature vane alloys. Second, the higher aluminum compositions are finding increased use as protective coatings. And, the NiCrAl's offer the potential for use in a variety of other gas turbine components. In high velocity oxidation tests these alloys have shown very good oxidation resistance. Figure 8 from ref. 7 shows that small weight losses occurred in tests to 500 hours at 1100° C under the severe thermal cycling conditions imposed by a sonic velocity combustion gas rig (one hour exposure cycles followed by airblast cooling). However, the alloys showing the least oxidation weight change

were generally the highest in aluminum content. As shown in figure 9, there appears to be a transition in ductility as indicated by the crack growth characteristics of these materials around 5% aluminum. Alloys below this level of aluminum develop thermal fatigue cracks about one 1/2 to 1/3 the length of those observed in alloys with aluminum contents over 5%. This is also seen in figure 10 where the three bars at the left all have compositions below the 5% aluminum level and the three deeply cracked bars to the right all have aluminum contents above that level.

The NiCrAls are also used as protective coatings because of good thermal fatigue resistance. In thermal cycling, substrate microstructure, however, has been shown to exert a major influence on life (ref. 8). Figure 11 and Table II show the results of cycling randomly cast alloys; the same alloys with an aluminide coating; some of the same alloys directionally solidified (DS); and DS alloys with NiCrAl overlay coatings. Note that TAZ8A, a NASA developed nickel base alloy (nominally Ni-8Ta-6Cr-6Al-4Mo-2.5Cb-1Zr-0.1C, has extremely good resistance to thermal fatigue cracking. And aluminide coatings increase the number of cycles before crack initiation of randomly cast materials. A major gain, however, is made by directional solidification and these benefits are extended another factor of two by the application of a physical vapor deposited NiCrAl coating. Thus, in the case of MM 200, the microstructural change and the coating combine to increase the cycles to first crack from 15 to approximately 6,500.

Large improvements in coating composition and substrate compatibility have been made under NASA programs. The 1090° C oxidation and thermal fatigue resistance of the aluminized ductile NiCrAl alloy coating patented by NASA (ref. 10) was reported at the 1974 conference. That coating concept has been evaluated on a variety of substrates. Figure 12 (ref. 11) shows that at 1200° C on a gamma-gamma prime delta directionally solidified substrate the aluminized NiCrAl coating offers some improvement over NiCrAlY alone. On that low thermal expansion (40 v/o Ni_3Cb) substrate, however, an even more protective system was identified in which the NiCrAlY surface was coated with Pt.

Finally, cermets of NiCrAlY with 5 to 20 v/o M_gO have shown cyclic furnace oxidation resistance comparable to NiCrAlY alloys without oxide additions for a number of special applications in an engine. The 1200° C weight change behavior of these cermets, over a 90 hour exposure, is shown in figure 13. Here only the 40 v/o M_gO material suffered large weight losses. Post test microstructures show little evidence of oxidation attack. And electron microscopic examination of the oxide particle/matrix alloy interfaces indicated excellent bonding and compatibility.

HOT CORROSION

NASA's fundamental studies of hot corrosion mechanisms include thermodynamic studies (for example, ref 13) in which the deposition of sodium sulfate from flames was examined. This deposition of sodium sulfate from flames containing sodium and sulfur is regarded as one of the fundamental steps in the phenomenon of hot corrosion of turbine components. An equilibrium thermodynamic description of the role of sodium and sulfur and other elements leading to the formation of condensed Na_2SO_4 useful in understanding the initial important stages of the corrosion mechanism. Reliable thermodynamic data are, of course, required for all of the important molecular species.

Until recently, the mode of vaporization of Na_2SO_4 had not been well understood. In the present work, gaseous species over liquid Na_2SO_4 have

been identified by the technique of high temperature molecular beam mass spectrometry. Typical spectra are shown in figure 14. The Na_2SO_4 gaseous molecule was positively identified and vapor pressures and other thermodynamic data were obtained for the system.

The thermodynamic properties of gaseous and condensed Na_2SO_4, along with additional pertinent species, were used in a NASA computer program to calculate equilibrium flame compositions and temperatures for representative turbine engine and burner rig flames. The results of such a calculation are shown in figure 15. The major conclusions to be drawn from the flame composition calculations are that: 1) Na_2SO_4 can be formed in the flame as either a condensed phase or as a gas; 2), that its formation is strongly dependent on the temperature of the flame as dictated by the fuel/oxidant ratio; and 3), that over most of the range of flame temperatures, NaCl, NaOH, or Na are the major Na-containing species. Temperatures for condensation of Na_2SO_4 (see fig. 16) were obtained as a function of sulfur and sea salt concentration to determine whether or not Na_2SO_4 would deposit from turbine or burner rig flames either in the combustion zone itself or downstream on components at lower temperatures. Additional work is underway on the thermochemistry of sodium sulfate formation kinetics and deposition mechanisms and parameters. The ultimate goal of these efforts to allow accurate prediction of deposition under burner rig and gas turbine conditions. This, it is hoped, will lead the way to relating burner rig and engine testing in a meaningful way.

In the area of coatings for hot corrosion resistance, three alloys each coated with two different aluminide coatings were evaluated by Mach 0.3 burner rig tests at 900° C - 5 ppm ASTM sea salt levels using both 10-minute and 1-hour cycles (ref. 14). Failure was defined as that time when local coating breakdown reached 0.050 in. in diameter. The results of these tests are shown in table III. These results indicate that total exposure time is the dominant consideration and that in these tests, time to failure is relatively insensitive to the number of exposure cycles. The time to failure divided by coating thickness was nearly constant for all coatings examined. Also, the time to coating failure, for any particular coating, was relatively insensitive to the substrate to which it had been applied.

Another potential way of minimizing hot corrosion attack is by the introduction of additives into the turbine fuel. Using a commercial chromium-based fuel additive at the 300 ppm level, accelerated hot corrosion tests were conducted at 900° C - 5 ppm sea salt, 1-hour cycles and the soluble salts were washed off the specimens every 10 cycles (ref. 15). Four uncoated nickel and cobalt based turbine airfoil alloys were evaluated in oxidation only (no additive, no sea salt), in hot corrosion (sea salt, no additive), and in hot corrosion with the fuel additive. The four alloys were IN-100, IN-792, IN-738, and MM509. The results of these tests are shown in figure 17. The fuel additive reduced weight losses by about a factor of two in all cases. However, in all cases significant hot corrosion attack was still observed.

The weight loss reductions due to the presence of the additive were about the same regardless of the chemistry of the alloys exposed.

Alloy modification is a third way to minimize hot corrosion. The benefits to alloy oxidation resistance of small silicon additions was reported to this group at the last conference. Such silicon additions also have a somewhat beneficial effect on hot corrosion as shown in figure 18 (ref. 16) for tests at 900° C, at Mach 1, and in 5 ppm, sea salt. However, mechanical property losses did occur when silicon compositional modifications were made and aluminide coatings offered substantially better protection in these tests.

CONCLUDING REMARKS

In this paper, highlights of NASA Lewis research efforts in oxidation and hot corrosion have been briefly described. Work in these areas continues with special emphasis on programs to integrate our knowledge of oxidation and hot corrosion behavior into life prediction techniques. It is hoped, that these studies will eventually allow estimates of lifetimes for hot turbine components operating in a wide variety of hostile environments.

REFERENCES

1. Spera, David A; and Grisaffe, Salvatore J.: Life Prediction of Turbine Components: On-Going Studies at the NASA Lewis Research Center, NASA TM X-2664, 1973.

2. Lowell, C. E.; Levine, S. R.; and Grisaffe, S. J.: Environmental Effects and Surface Protection of High Temperature Alloys: A Review of NASA Lewis Programs. Proceedings of the 1974 Gas Turbine Materials in the Marine Environment Conference, John W. Fairbanks and Irving Machlin eds., NCIC-75-27, Metals and Ceramics Infor. Ctr., 1974, pp. 535-554.

3. Barrett, Charles A.; and Pressler, Alden E.: COREST: A Fortran Computer Program to Analyze Paralinear Oxidation Behavior and its Application to Chromic Oxide Forming Alloys. NASA TN D-8132, 1976.

4. Deadmore, Daniel L.; and Lowell, Carl E.: The Effect of ΔT (Oxidizing Temperature Minus Cooling Temperature) on Oxide Spalling, NASA E-8830.

5. Lowell, Carl E.; Garlick, Ralph G.; and Henry, Bert: Thermal Expansion in the Ni-Cr-Al and Co-Cr-Al Systems to 1200° C Determined by High-Temperature X-Ray Diffraction. Met. Trans. vol. 7A, no. 5, May 1976, pp. 655-660.

6. Barrett, Charles A.; and Lowell, Carl E.: Resistance of Nickel-Chromium-Aluminum Alloys to Cyclic Oxidation at 1100° and 1200°. NASA TN D-8255, 1976.

7. Deadmore, Daniel L., Lowell, Carl E., and Santoro, Gilbert J.: High Gas Velocity Oxidation and Hot Corrosion Testing of Oxide Dispersion-Strengthened Nickel-Base Alloys. NASA TM X-71835, 1975.

8. Bizon, Peter T.; and Spera, David A.: Comparative Thermal Fatigue Resistance of Twenty-Six Nickel- and Cobalt-Base Alloys. NASA TN D-8071, 1975.

9. Waters, William J.; and Freche, John C.: A High Strength Nickel-Base Alloy with Improved Oxidation Resistance up to 2200° F. ASME Paper 67-GT-T, Mar. 1967.

10. Gedwill, Michael A.; and Grisaffe, Salvatore J.: Duplex Aluminized Coatings. U.S. Patent 3,869,779, Mar. 11. 1975.

11. Felten, E. J.; Strangman, T. E., and Ullon, N. E.: Coatings for Directional Eutectics. (PWA-5091, Pratt and Whitney Aircraft; NAS3-16792), NASA CR-134735, 1974.

12. Zaplatynsky, Isidor: Effect of Magnesium Oxide Content on Oxidation Behavior of Some Superalloy-Base Cermets. NASA TM X-3265, 1975.

13. Kohl, F. J., Stearns, C. A.; and Fryburg, G. C.: Sodium Sulfate: Vaporization Thermodynamics and Role in Corrosion Flames. International Symposium on Metal-Slag-Gas Reactions and Processes, by Z. A. Foroulis and W. W. Smeltzer, eds., The Electrochemical Soc., 1975, pp. 649-664.

14. Santoro, Gilbert J.: Hot Corrosion Evaluation of Aluminide Coated Superalloys in Support of an ASTM Round Robin Program. NASA TM X-71734, 1975.

15. Lowell, Carl E.; and Deadmore, Daniel L.: The Effect of a Chromium Containing Fuel Additive on Hot Corrosion, NASA TM X-73465, 1976.

TABLE I. - THERMAL EXPANSION OF Ni-Cr-Al ALLOYS

Alloy, at. %	Phase											
	γ/γ'				β				α-Cr			
	Lattice parameter at 25° C, $LP_{25^{\circ}C}$, nm	Expansion constant, R	Mean coefficient of thermal expansion, CTE, $^{\circ}C^{-1}$	Standard deviation of lattice parameter, σ_{LP}	Lattice parameter at 25° C, $LP_{25^{\circ}C}$, nm	Expansion constant, R	Mean coefficient of thermal expansion, CTE, $^{\circ}C^{-1}$	Standard deviation of lattice parameter, σ_{LP}	Lattice parameter at 25° C, $LP_{25^{\circ}C}$, nm	Expansion constant, R	Mean coefficient of thermal expansion, CTE, $^{\circ}C^{-1}$	Standard deviation of lattice parameter, σ_{LP}
Ni-13Cr-12Al	0.3557	20.6×10^{-4}	20×10^{-6}	0.14×10^{-2}	------	---------	-------	---------	------	---------	-------	---------
Ni-18Cr-11Al	.3563	20.5	20	.10	------	---------	-------	---------	------	---------	-------	---------
Ni-16Cr-6Al	.3545	18.6	18	.07	------	---------	-------	---------	------	---------	-------	---------
Ni-16Cr-6Al[a]	.3551	19.3	19	.09	------							
Ni-10Cr-17Al	.3561	20.5	20	.23	------							
Ni-16Cr-18Al	.3573	19.8	19	.12	0.2851	18.7×10^{-4}	18×10^{-6}	0.10×10^{-2}	------	---------	-------	---------
Ni-12Cr-26Al	.3574	19.8	19	.19	.2864	17.9	17	.17	------	---------	-------	---------
Ni-12Cr-23Al	.3574	19.4	19	.08	.2852	18.4	18	.07	------	---------	-------	---------
Ni-14Cr-24Al	.3574	17.6	17	.16	.2845	22.5	22	.03	------	---------	-------	---------
Ni-14Cr-24Al[a]	.3578	16.9	17	.28								
Ni-21Cr-17Al	.3572	20.5	20	.24	.2853	19.9	20	.06	------	---------	-------	---------
Ni-19Cr-24Al	.3574	17.9	17	.11	.2862	19.1	19	.46	0.2860	13.9×10^{-4}	13×10^{-6}	0.20×10^{-2}
Ni-19Cr-27Al	.3572	17.9	18	.14	.2860	20.6	20	.17	.2880	13.2	13	.06
Ni-17Cr-29Al	------	---------	-------	---------	.2855	22.4	22	.20	.2879	13.1	13	.05
Average	------	19.4	-------	---------	------	19.9	------	---------	------	13.4	-------	---------

[a]Replicate specimens.

TABLE II. - CYCLES TO CRACK INITIATION

[DS indicates that the alloy was cast with a directionally solidified grain structure.]

Alloy	Bed temperatures[a]			
	1088° and 310° C (1990° and 600° F)		1129° and 357° C (2065° and 675° F)	
	Cycles	Specimen design (fig. 1(a))	Cycles	Specimen design (fig. 1(a))
NASA TAZ-8A + RT-XP coat	12 500	B		
Mar-M 200 DS + NiCrAlY overlay	4 500	C		
	8 500	C		
NASA TAZ-8A DS + NiCrAlY overlay	4 500	B		
	6 500	B		
NX 188 DS + RT-1A coat	5 100	B	>6100	B
	5 100	B		
NASA TAZ-8A DS	4 350	B	1200	B
	4 350	B		
	6 500	B		
NX 188 DS	4 350	B	5125	B
	4 350	B		
Mar-M 200 DS	1 250	C	1200	C
	1 750	C		
	4 700	A		
IN 100 DS + Jocoat	2 400	A	1950	C
IN 100 DS	2 400	A	1200	C
NASA WAZ-20 DS + Jocoat	1 750	B	1350	B
	1 750	B		
B 1900 + Hf + Jocoat	585	B	1550	B
	2 375	B		
B 1900 + Jocoat	1 190	A	1050	C
			>1200	C
NASA TAZ-8A	600	A	450	C
	800	C		
NX 188 + RT-1A coat	300	B	200	B
	800	B		
X 40	600	A	150	C
B 1900	400	A		
IN 162	400	A		
IN 100 + Jocoat	[b]400	A	38	C
TD NiCr	250	A	13	C
IN 713C	250	A		
Mar-M 509	238	B	[b]150	B
NX 188	100	B	50	B
	238	B		
NASA VI-A	138	B	[b]38	B
NASA WAZ-20 + Jocoat	100	B	13	B
	138	B		
Rene 80	100	B	50	B
IN 738	100	B	50	B
RBH	100	B	50	B
Mar-M 302	75	A		
U 700 cast	75	A		
WI 52	75	A		
IN 100	38	A		
Mar-M 200 + Jocoat	25	C	[b]13	C
Mar-M 200	13	A		
U 700 wrought	13	A		
M 22	13	A		

[a]3-minute immersion in both heating and cooling fluidized beds.

[b]1.02-millimeter (0.040-in.) radius edge failure.

TABLE III. - FAILURE TIMES OF COATED ALLOYS

Specimen	Time to failure hours (cycles)			Specific time to failure* hours per micron		
	Ten minute cycles (duplicate runs)		One hour cycles	Ten minute cycles (duplicate runs)		One hour cycles
IN-713C						
Coating A	60 (360)	70 (420)	60 (60)	0.7	0.8	0.6
Coating B	45 (270)	55 (330)	70 (70)	0.5	0.7	0.8
IN-100						
Coating A	40 (240)	40 (240)	30 (30)	0.5	0.6	0.3
Coating B	40 (240)	45 (270)	55 (55)	0.6	0.7	0.7
B-1900						
Coating A	55 (330)	55 (330)	55 (55)	0.6	0.7	0.6
Coating B	40 (240)	40 (240)	45 (45)	0.6	0.7	0.9

*Time to failure divided by the initial coating thickness.

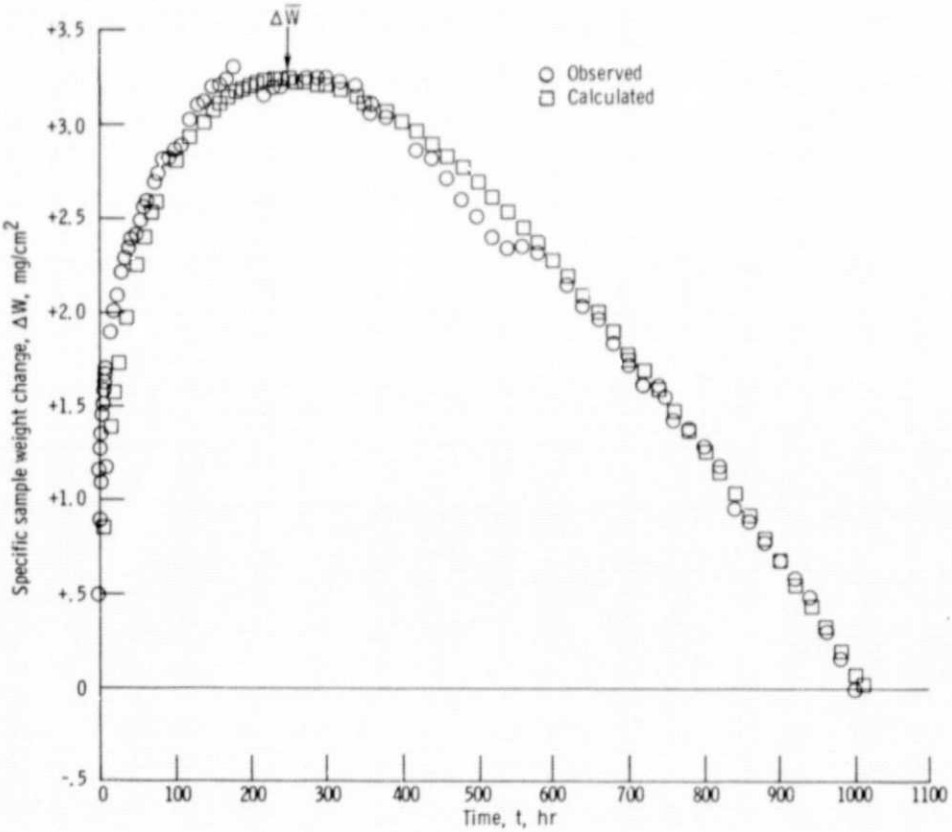

Figure 1. - Specific sample weight change ΔW observed and calculated by paralinear analysis (CORES1) for Cr_2O_3-forming alloy Ni-40Cr at 1200° C. Maximum specific sample weight change in paralinear oxidation, $\Delta\bar{W}$, 3.24 mg/cm^2; time to reach $\Delta\bar{W}$, $\bar{t}$, 250 hr; error estimate, 0.243 mg/cm^2; type 1 input.

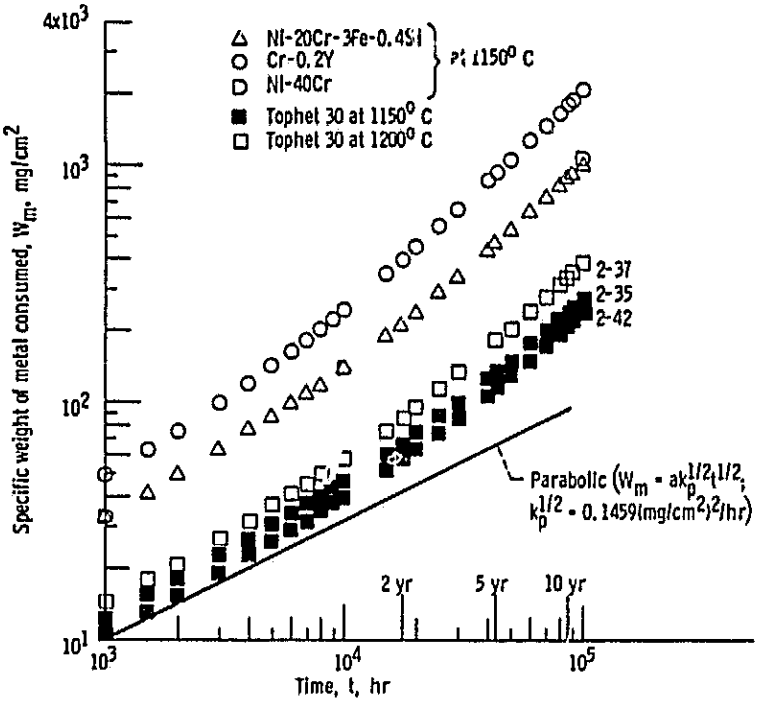

Figure 2. - CORREST-calculated specific weight of metal consumed W_m for predominantly Cr_2O_3-forming alloys above 1100° C, assuming parallinear oxidation. Stoichiometric constant, a, 2.1667.

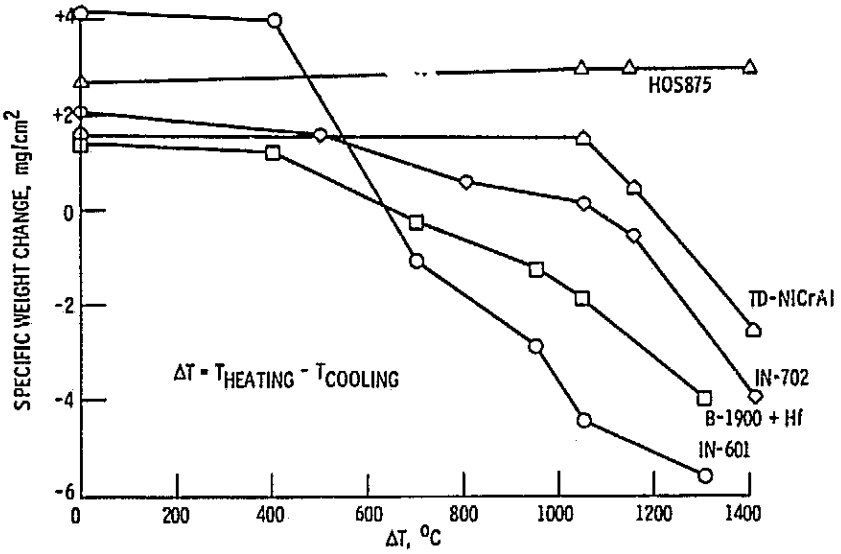

Figure 3. - Effect of ΔT on oxide spalling.

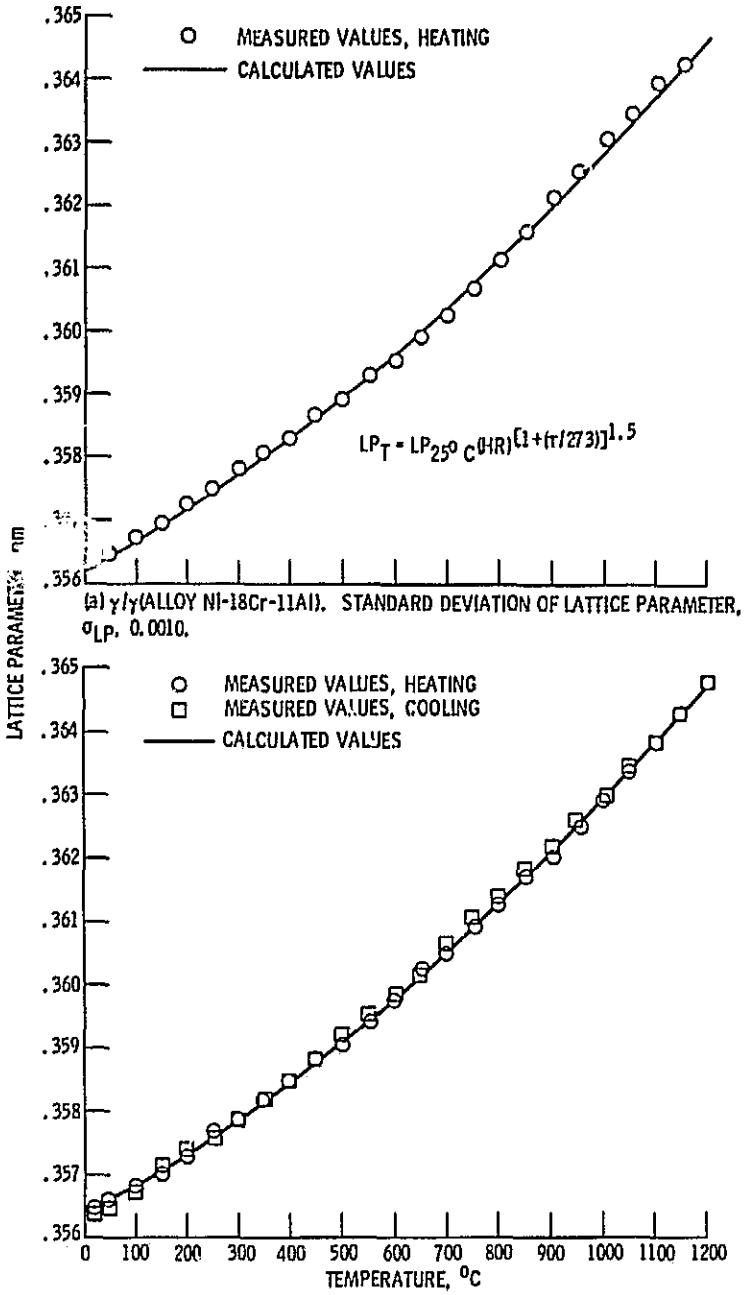

(a) γ/γ'(ALLOY Ni-18Cr-11Al). STANDARD DEVIATION OF LATTICE PARAMETER, σ_{LP}, 0.0010.

(b) α-Co (ALLOY Co-13Cr-12Al). STANDARD DEVIATION OF LATTICE PARAMETER, σ_{LP}, 0.0007.

Figure 4. - Typical expansion curves in the Ni-Cr-Al and Co-Cr-Al systems.

General specific weight change equation

(1) $\Delta w/A = k_1^{1/2} t^{1/2} - k_2 t \pm \sigma$

Attack parameter

(2) $Ka = k_1^{1/2} + 10\, k_2$

Fourth order regression equation

(3) $\log Ka = a + b_1 Cr + b_2 Al + b_3 AlCr + b_4 Cr^2 + b_5 Al^2 + b_6 CrAl^2 + b_7 AlCr^2 + b_8 Cr^3 + b_9 Al^3 + b_{10} Cr^2 Al^2 + b_{11} Cr^3 Al + b_{12} CrAl^3 + b_{13} Cr^4 + b_{14} Al^4 \pm \sigma$

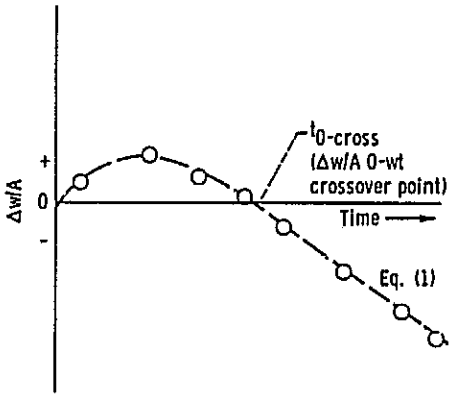

Figure 5. - Typical specific weight change as function of time curve for alloy with nearly uniform scale growth and scale spalling.

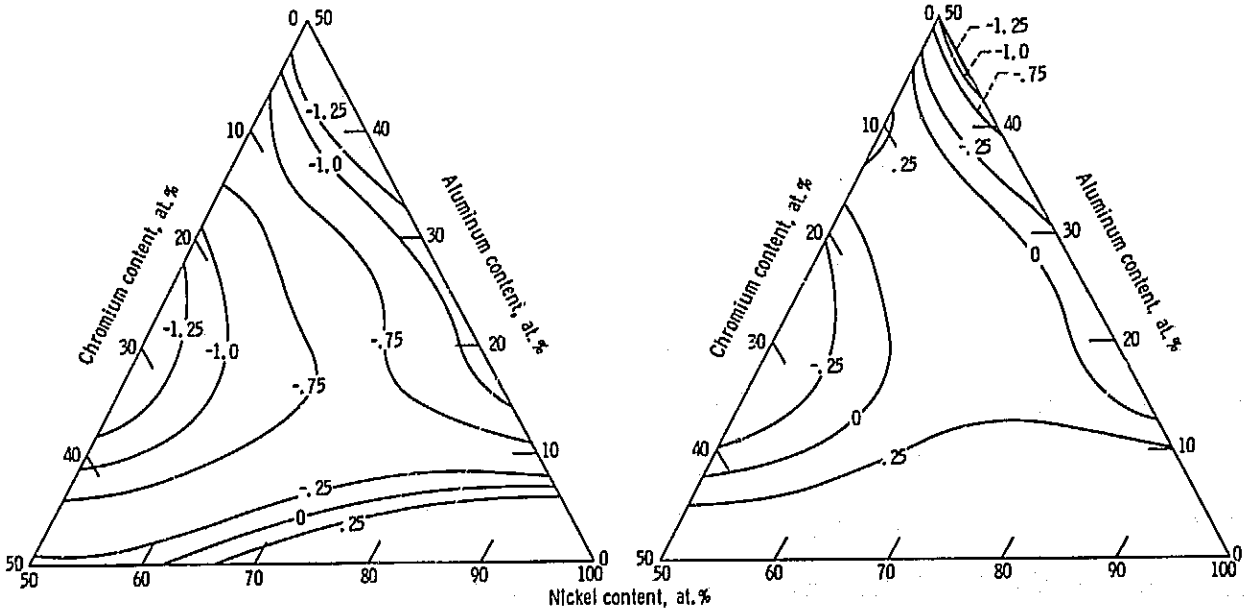

(a) For alloys melted in zirconia crucibles.

(b) For alloys not melted in zirconia crucibles.

Figure 6. - Attack contours in Ni-50Cr-50Al system at 1100° C.

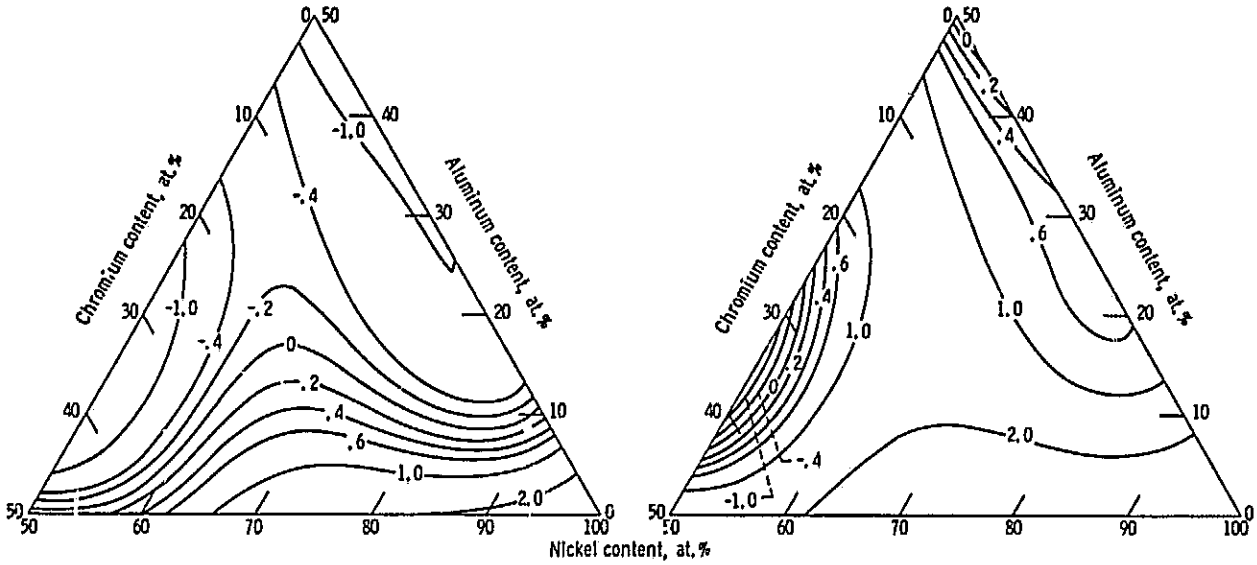

(a) For alloys melted in zirconia crucibles.

(b) For alloys not melted in zirconia crucibles.

Figure 7. - Attack contours in Ni-50Cr-50Al system at 1200° C.

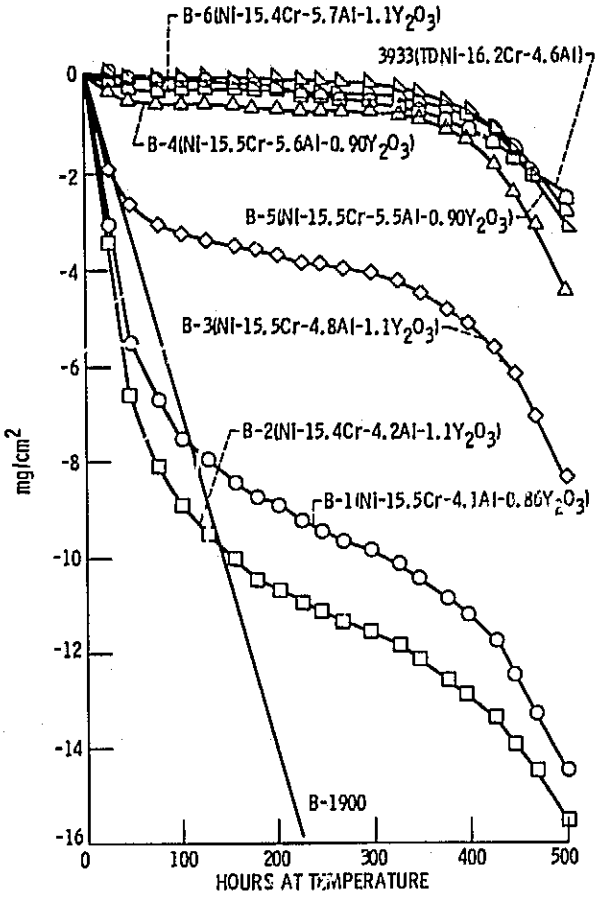

Figure 8. - Mach 1 oxidation of dispersion strengthened NiCrAl alloys at 1100° C. A-1 fuel; 1 hour cycles.

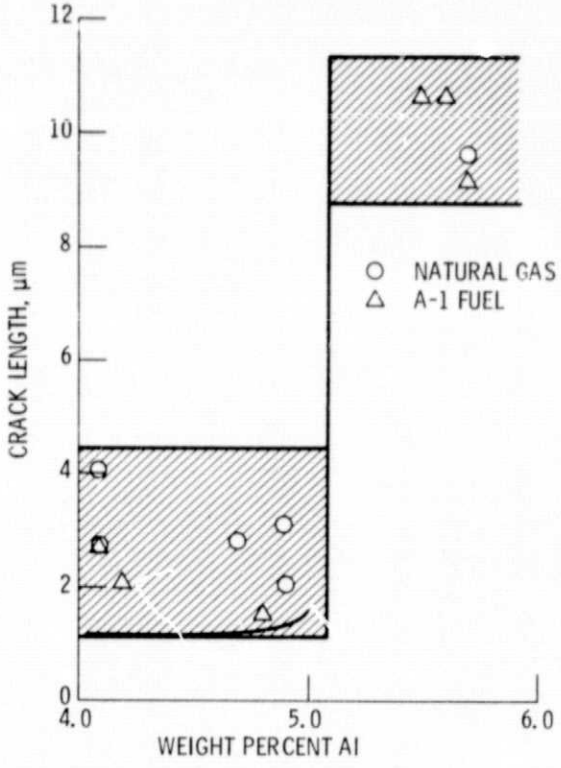

Figure 9. - Effect of aluminum content on the maximum thermal fatigue crack length of some YD-NiCrAl alloys, 500 - one hour cycles at 1100° C in Mach 1 gases.

Figure 10. - Thermal fatigue cracks in some dispersion strengthened NiCrAl alloys. Run was 500 - 1 hour cycles at 1100° C in mach 1 gases.

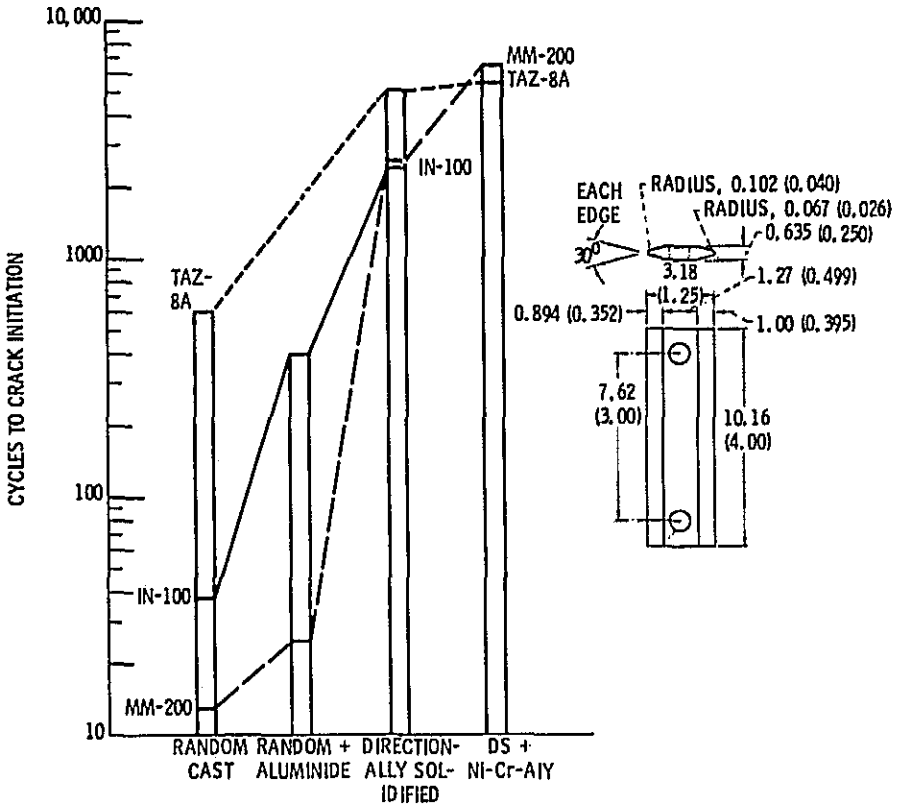

Figure 11. - Effect of directional solidification and coatings on crack initiation in fluidized bed thermal fatigue cycle; 1090° C, 3 minutes to 320° C, 3 minutes.

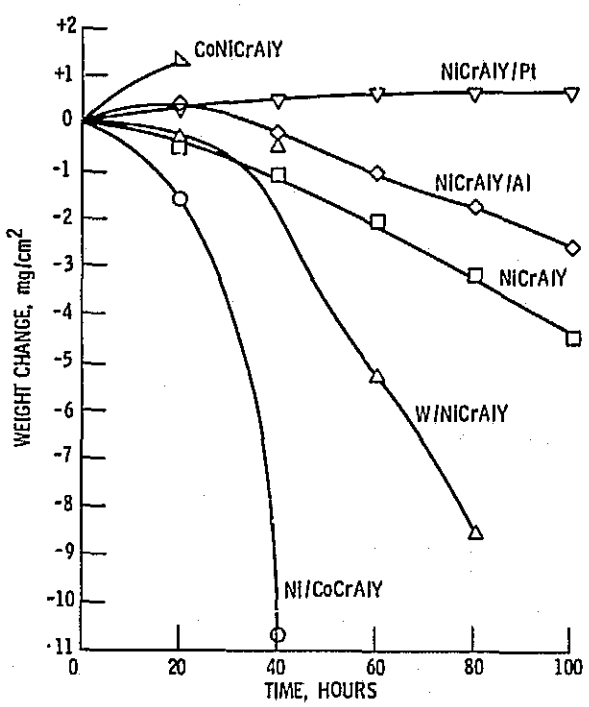

Figure 12. - 1478° K (2200° F) cyclic oxidation behavior of eutectic alloy coupons coated with vapor deposited overlay coatings.

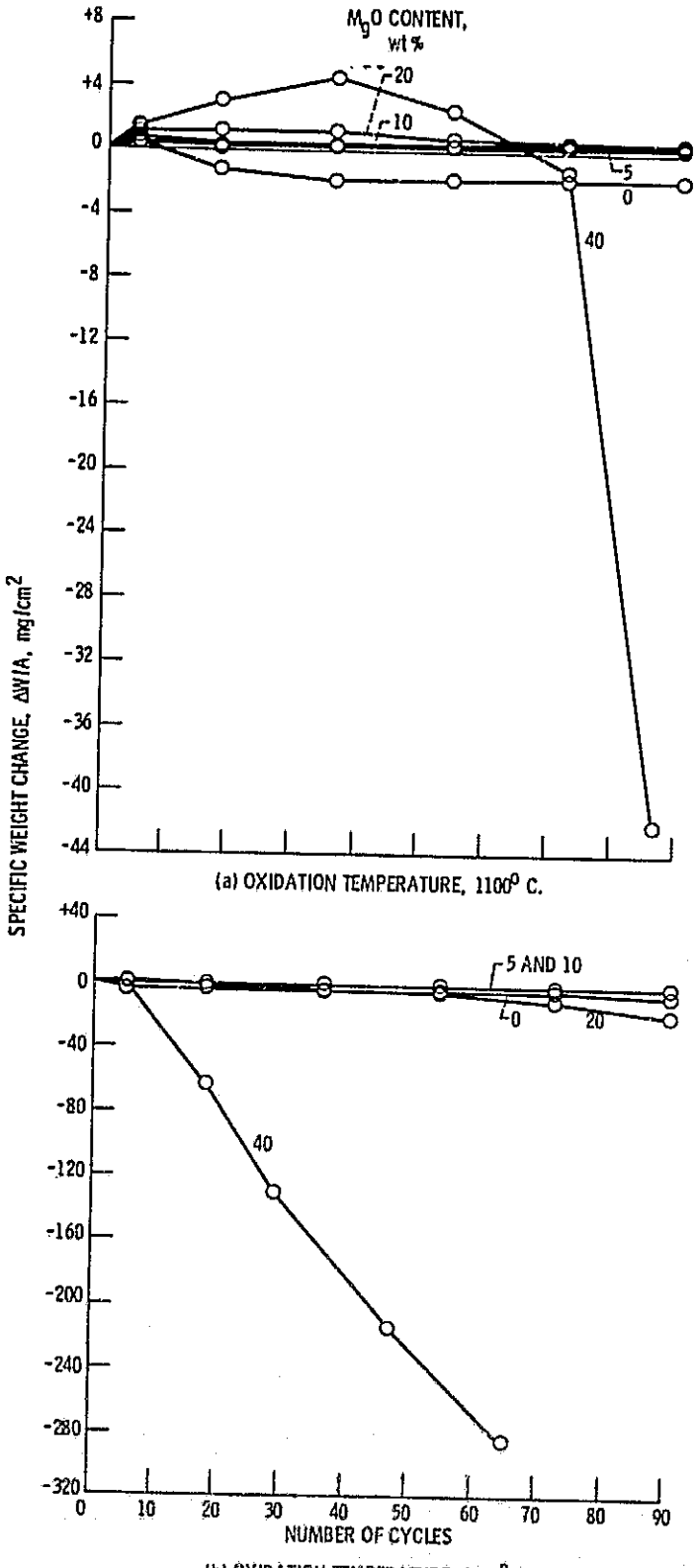

Figure 13. - Sample specific weight change of NiCrAlY alloy and MgO + NiCrAlY cermets as function of number of 1-hour cycles in still air.

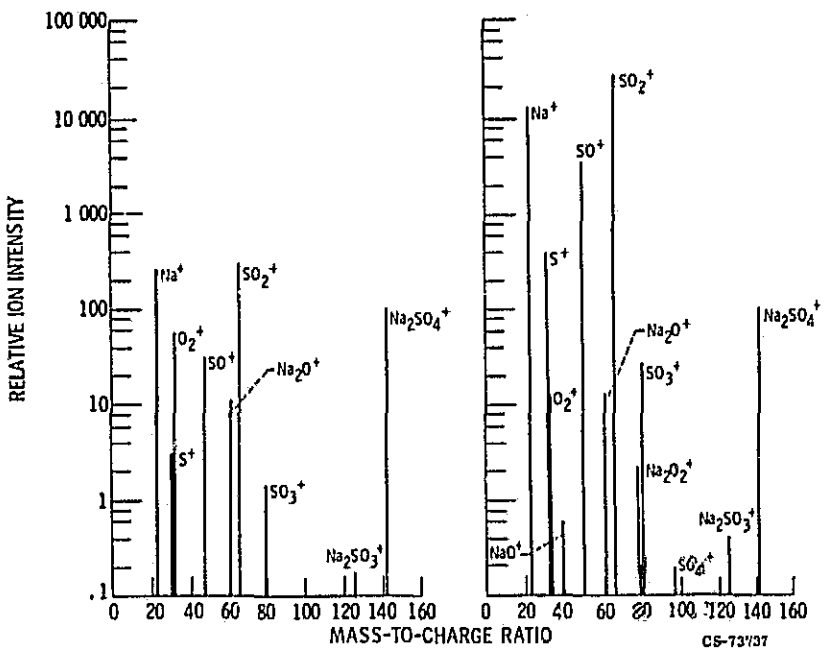

(a) 1370 K IN A PLATINUM CELL OR AN Al_2O_3 LINER IN A PLATINUM CELL.

(b) 1380 K IN A ZrO_2 LINER IN A TUNGSTEN OR TANTALUM CELL.

Figure 14. - Mass spectra of vapors over $Na_2SO_4(l)$ at 30 electron volts ionizing energy.

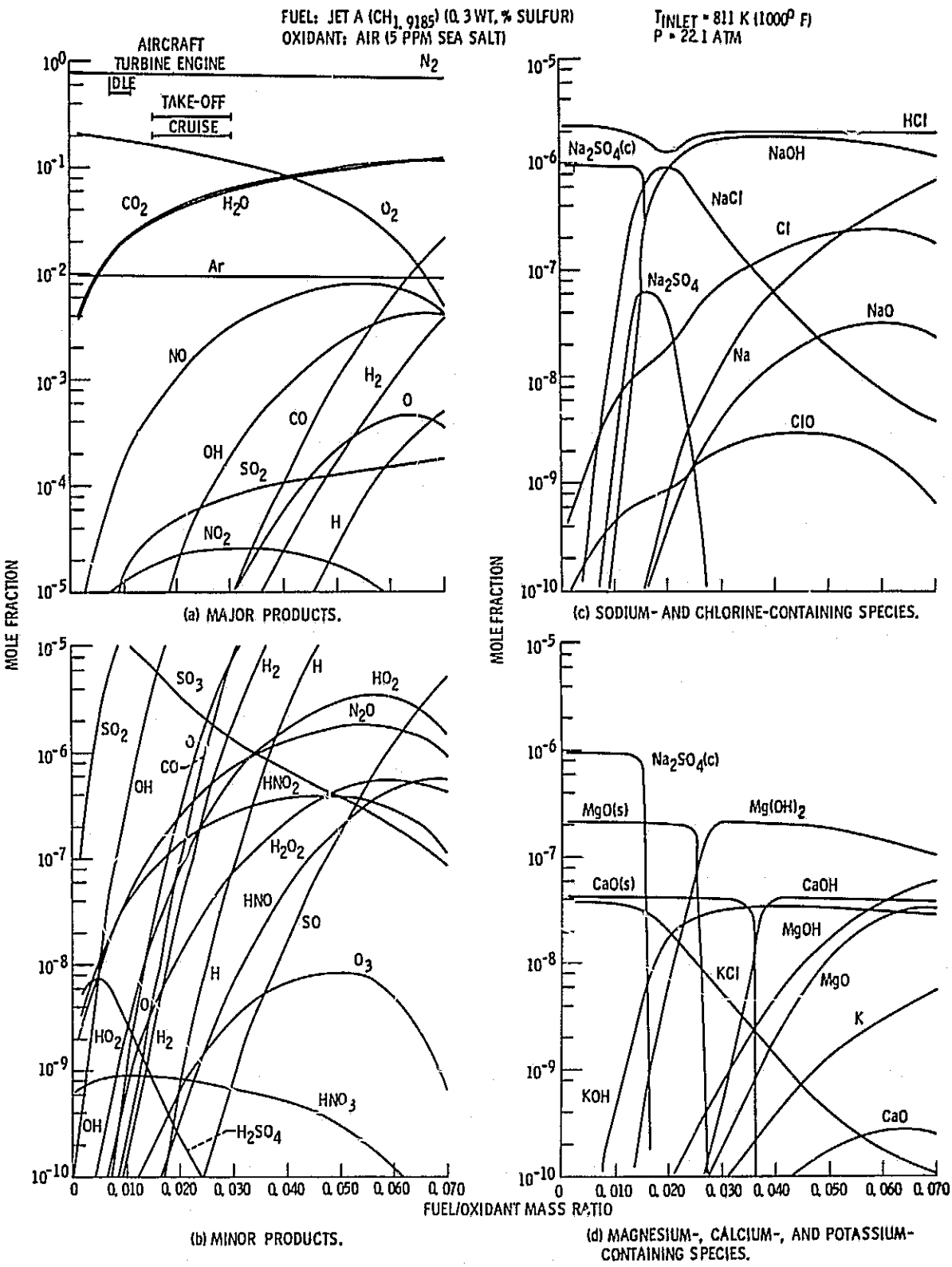

Figure 15. - Equilibrium chemical composition of flame gas versus fuel/oxidant mass ratio characteristic of an aircraft turbine engine with sulfur in the fuel and sea salt in the oxidant.

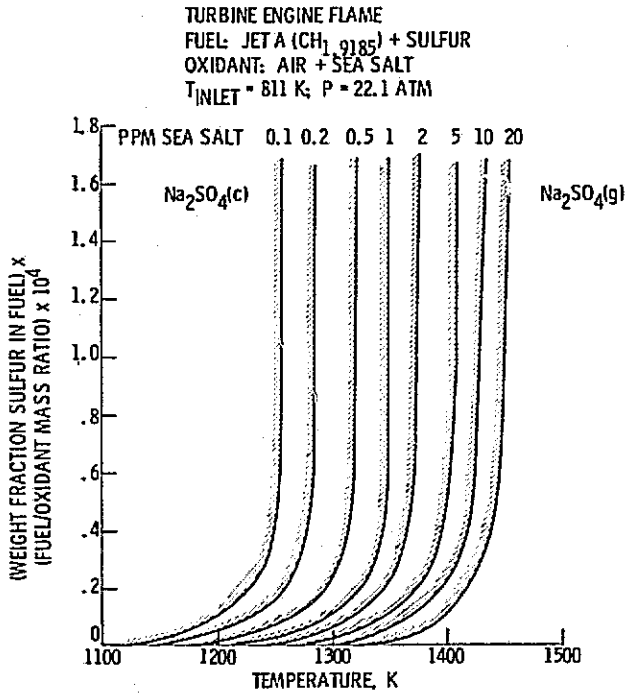

Figure 16. - Condensation temperature of Na_2SO_4 as a function of sulfur content and amount of fuel and sea salt concentration in oxidant for an aircraft turbine engine flame.

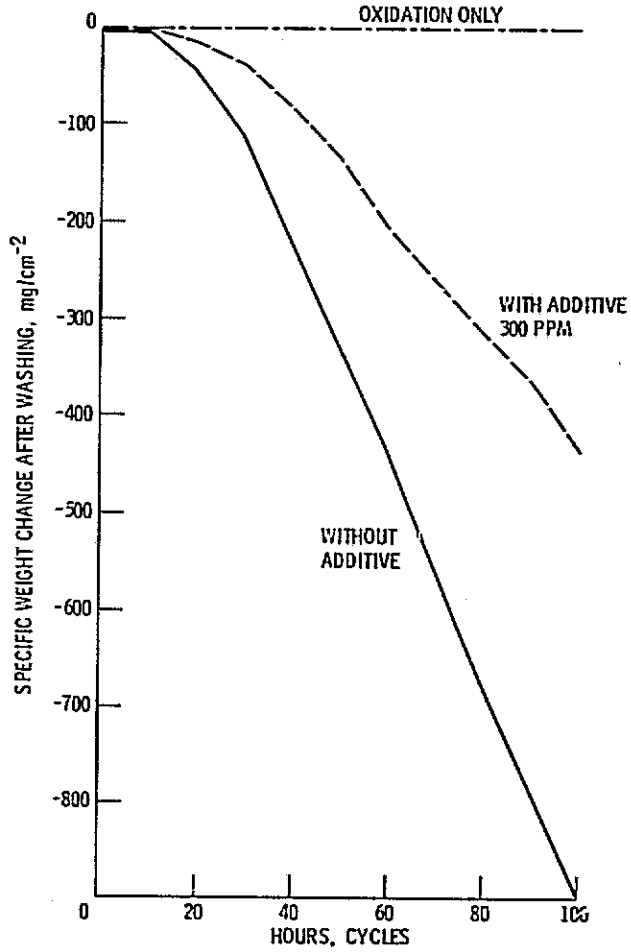

(a) IN-100.

Figure 17. - Effect of Cr additive on hot corrosion at 900° C; one hour cycles, washed every 19 cycles, 5 ppm salt.

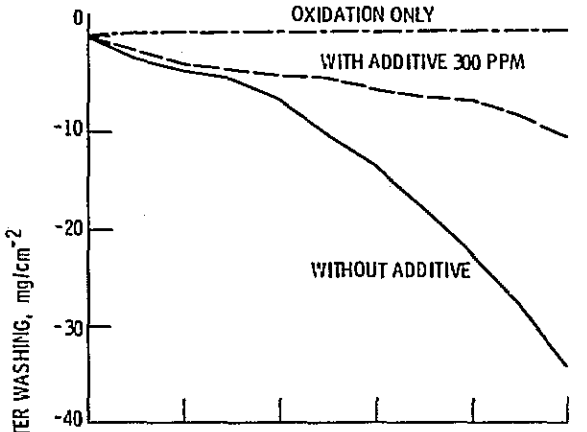

(b) IN-792.

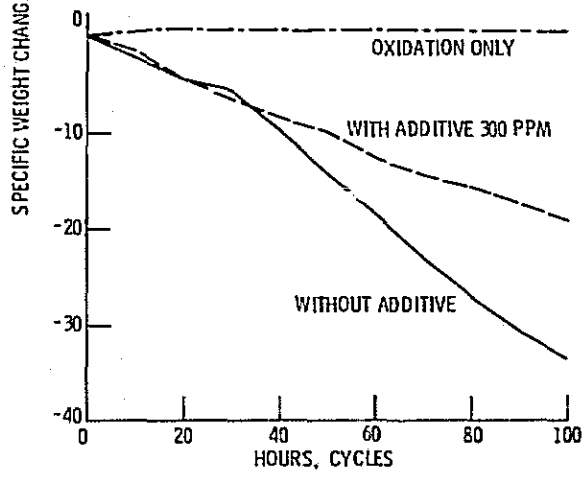

(c) IN-738.

Figure 17. - Continued.

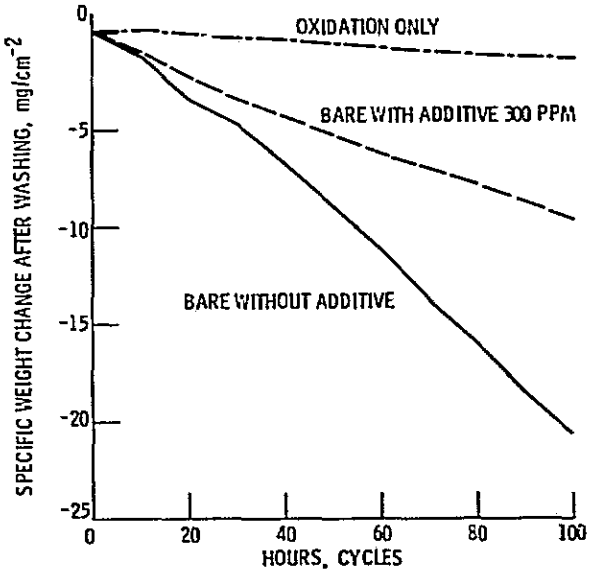

(d) MM509.

Figure 17. - Concluded.

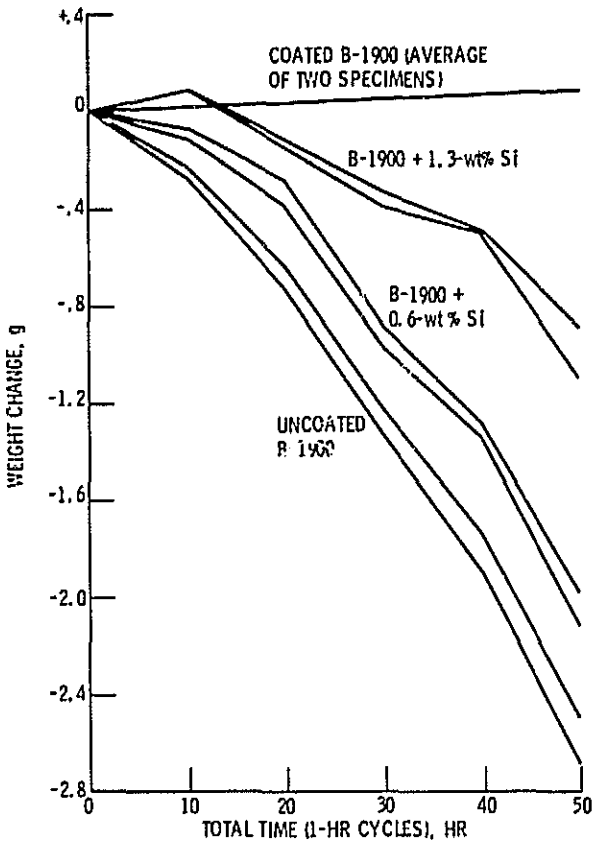

Figure 18. - Effect of silicon concentration on resistance of B-1900 to sulfidation in Mach 1 burner exhaust with 5-ppm salt at 900° C, compared with aluminide-coated B-1900. Cycle time, 1 hr; specimen weight, ~120 g.